JOURNAL OF AIRCRAFT
Vol. 45, No. 4, July–August 2008

Variable Fidelity Conceptual Design Environment for Revolutionary Unmanned Aerial Vehicles

Stephane Dufresne,* Carl Johnson,† and Dimitri N. Mavris‡
Georgia Institute of Technology, Atlanta, Georgia 30332-0150

DOI: 10.2514/1.35567

This paper describes the development of an unmanned aerial vehicle's conceptual design environment. A review of current unmanned aerial vehicle design challenges is conducted, which leads to the description of the desired capabilities for the environment. The key characteristics of the design environment include the capability of integrating variable fidelity, modular, and flexible disciplinary analysis tools. The environment is tested against available data from the AeroVironment Pathfinder Plus vehicle. In addition to the Pathfinder Plus mission analysis, aerodynamics, propulsion, and structures performance results are discussed and then applied to a hurricane-tracker mission. This case study demonstrates the environment's capability to perform and explore new types of missions. A further exploration of the Pathfinder Plus design space is conducted using response surface methodology. This investigation provides valuable information regarding design tradeoffs, which are essential for the selection of a final vehicle architecture.

Nomenclature

AR	=	wing aspect ratio
C_D	=	vehicle drag coefficient
$C_{\mathrm{DF_P}}$	=	pods friction drag coefficient
$C_{\mathrm{DF_W}}$	=	wing friction drag coefficient
C_{Di}	=	vehicle-induced drag coefficient
C_{Dm}	=	vehicle miscellaneous drag coefficient
C_d	=	airfoil drag coefficient
C_L	=	vehicle lift coefficient
Cl	=	airfoil lift coefficient
$C_{l\text{-max}}$	=	airfoil maximum lift coefficient
D	=	vehicle drag, N
ezV	=	electrolyzer voltage, V
E_{ez}	=	solar energy consumed to power the electrolyzer, W
$\bar{E}_{\mathrm{ez}}$	=	energy consumed by the electrolyzer per mass of hydrogen, W/kg
E_{fc}	=	total fuel cell energy production, W
$\bar{E}_{\mathrm{fc}}$	=	energy produced by the fuel cell per mass of hydrogen, W/kg
E_{solar}	=	solar energy consumed to power the vehicle, W
E_{total}	=	total energy consumed to power the vehicle, W
fcV	=	fuel cell voltage, V
Kv	=	voltage constant
$kgH2$	=	mass of hydrogen, kg
m_{prop}	=	total propulsion system mass, kg
n_{days}	=	number of days the vehicle flew
S	=	wing planform area, m^2
sa_{eff}	=	solar cell efficiency
T_A	=	thrust available, N
R	=	response of the response surface equation
V	=	vehicle velocity, m/s
W_i	=	vehicle actual weight, N
$Wpld$	=	payload mass, kg
x_i	=	design variable of the response surface equation
β_ι	=	coefficients of the response surface equation
η_{ez}	=	electrolyzer efficiency

Received 8 November 2007; revision received 1 February 2008; accepted for publication 29 February 2008.

*Graduate Research Assistant, Aerospace Systems Design Laboratory, Daniel Guggenheim School of Aerospace Engineering. Member AIAA.

†Graduate Research Assistant, Aerospace Systems Design Laboratory, Daniel Guggenheim School of Aerospace Engineering. Member AIAA.

‡Boeing Professor of Advanced Aerospace Systems Analysis and Director of Aerospace Systems Design Laboratory, Daniel Guggenheim School of Aerospace Engineering. Associate Fellow AIAA.

I. Introduction

THE revenue of the global unmanned aerial vehicle (UAV) market in 1998 was $2.07 billion. In 2008, the forecast for the same market is $6.87 billion, a growth of more than 300% in 10 yr [1]. In 2003, the market for UAVs performing reconnaissance and surveillance missions was expected to be worth more than $10 billion over the next decade.§ The visibility and success of UAV military applications in Afghanistan and Iraq have greatly contributed to the market growth. The Department of Defense justifies the need for UAVs over manned aircraft when a mission includes operations that can be qualified as "dull" (long duration), "dirty" (sampling of hazardous material), or "dangerous" (extreme exposure to hostile action) [2]. The same justifications can also be applied to civilian applications such as the communication relay station, hurricane tracking, search and rescue in a hostile environment, and wildfire monitoring. Most of these applications involve the development and integration of new technologies that make UAVs revolutionary.

The ability to test and integrate new technologies is a major factor in the expansion of the UAV market. For instance, the increase in fuel price favors a push toward more electric aircraft. In this context, many researchers are trying to use fuel cell systems as primary and secondary sources of power [3–6]. The NASA Aerial, Regional-Scale Environmental, Survey of Mars (ARES) UAV platform is another example of a technology demonstrator [7–9]. It is designed to fly in the Martian atmosphere while analyzing Mars's crustal magnetism and the atmosphere boundary layer composition. Consequently, based on the latest UAV development and applications, the expansion of the UAV market opens the path for the development of more complex vehicles.

As the complexity of the UAV systems is increasing, physical prototypes are getting more expensive, making virtual modeling and prototyping more attractive. The design of virtual prototypes is conducted using analysis tools with different levels of fidelity. Low fidelity tools are used to explore the design space whereas high fidelity tools are used to refine the performance predictions of a specific vehicle design. A design environment integrates multiple

§Data available online at http://www.forecastinternational.com/press/release.cfm?article=41 [retrieved 30 April 2007].

disciplinary tools in a common framework. A partial list of currently available design environments for fixed wing aircraft includes the flight optimization systems (FLOPS) developed at NASA Langley Research Center [10], aircraft synthesis (ACSYNT) developed by the NASA Ames Research Center and Virginia Polytechnic Institute and State University [11,12], and the general aviation synthesis program (GASP) developed at the NASA Ames Research Center [13]. Lu et al. discussed the applications and limitations of these conceptual design environments and identified two major limitations [14]. The first limitation is that the applications of the design tools are generally limited to a specific type of vehicle, because the sizing algorithm is hard coded in the model, which also has the consequence of making it difficult to model a wide variety of missions. The second limitation is the lack of flexibility or scalability of the disciplinary analysis tools. Often, the aerodynamics and propulsion models are imbedded within the sizing algorithm, which makes it difficult to modify or change the analysis tool. The authors of [14] are focused on the first limitation; however, they did not fully address the scalability analysis issue, which is required for a variable fidelity environment.

The purpose of this paper is to demonstrate how the scalability limitation can be addressed through the use of flexible integration software and how to use the new capabilities to create a variable fidelity environment for the design of revolutionary UAVs. It should be noted that no rotorcraft or lighter-than-air vehicles are considered in the development of this environment; however, the same methodology could be used to model such vehicles.

This research paper is divided into six sections. The second section of this paper presents challenges relating to the creation of a UAV design environment. The third section introduces the design process and describes the UAV conceptual design environment, including the disciplinary tools and sizing strategies. The fourth section compares the design environment results with publicly available data from the AeroVironment Pathfinder Plus UAV. The fifth section demonstrates the capability of using an existing vehicle to perform new types of mission. More specifically, a hurricane-tracking platform is explored with different propulsion architectures. The last section presents the conclusions of this research and future work that will enhance the capabilities of the environment.

II. Unmanned Aerial Vehicle Design Challenges

There exist many different types of UAV platforms, from micro aerial vehicle (MAV) to high-altitude long-endurance aircraft (HALE) [15,16]. The fundamental differences in UAV size, shape, and operating conditions imply different sizing algorithms, performance analysis tools, and operational scenarios. The objective of this section is to discuss design environment and UAV analysis challenges.

The challenge of creating a flexible and modular design environment is in the coupling of operational and systems capabilities. The term capability is defined by Saleh et al. as "fundamental requirements of the system and [they] represent the features of functions of the system needed or desired by the customer" [17]. In the design environment, capabilities are connected to the systems through a set of disciplines. For instance, the endurance capability can be traced to the wing system through the aerodynamics analysis module. The most common aerospace disciplines included in aircraft design are aerodynamics, power, propulsion, structure, and control. The systems model represents a synthesis of disciplinary tools that provide the means to verify that a given UAV alternative can fulfill the desired customer requirements.

During the conceptual design phase of a new vehicle, a large number of alternatives is considered. The exploration of different systems alternatives can be achieved through a flexible and modular design environment [14]. For example, the design team may consider different propulsion architectures like an internal combustion engine with a propeller, a turbofan engine, a ducted fan, or a liquid hydrogen engine. Consequently, the design environment must be modular enough to integrate the various systems models and flexible enough to allow for the creation of scripts connecting the different systems. The proposed design environment can then be used as an enabler to explore the UAV power, aerodynamics, and structural challenges.

A UAV performing a surveillance mission (i.e., hurricane tracker) requires long range and endurance capabilities. This operational challenge depends on the fuel capacity and fuel consumption, and also requires an efficient power management system [18]. The power management is different for regenerative [19] and nonregenerative systems. For a nonregenerative concept, there is a fixed amount of energy being depleted until the system can no longer fly. For a regenerative system, such as a hydrogen fuel cell combined with an electrolyzer and solar panel, the level of energy is a function of the solar radiation at a specific aircraft orientation with respect to the sun. For this power architecture, the hydrogen is used as fuel by the fuel cell stacks whereas the solar panels provide an extra source of energy. The extra energy from the solar panels is used to electrolyze the water produced by the fuel cell. This process produces hydrogen and oxygen that are reused by the fuel cell stacks. Modeling the power management for the entire vehicle is a difficult challenge, primarily because it requires an almost complete power architecture, which is often not fully defined at the conceptual design phase.

The operation of UAVs at a wide range of altitude and Mach number presents an interesting aerodynamics modeling challenge. The dimensional scale of UAVs can be much smaller than conventional aircraft, which impacts the aerodynamics characteristics of the vehicle. The air viscosity effect, represented by the Reynolds number, varies drastically depending on the flight condition and the size of the vehicle, whereas the air compressibility effect, represented by the Mach number, strictly depends on the flight conditions. A great deal of research has been done on aerodynamic models including numerical lifting line [20–22], vortex lattice models [23],[¶] and applications of computational fluid dynamics (CFD) to UAV [24,25]. At the beginning of the design process, faster tools are required to help the down selection of alternatives. Once a configuration is selected, more accurate predictions of the performance are obtained through higher-fidelity models. Currently, in conceptual design, aerodynamics models are used separately and sequentially, from lower to higher fidelity. Combining the models in a unique environment allows the design team to perform their analyses using the same design variables within a common framework.

The design of fixed wing UAVs also presents significant structural analysis challenges. For instance, the prediction of aeroelastic characteristics is an important field of research [26]. This is especially true for flexible high-aspect-ratio wings studied in their application to high-altitude long-endurance aircraft [27,28]. Also, the use of morphing wings is actively being pursued for UAV design [29,30]. The morphing wings have a significant impact on the aerodynamic and operational characteristics of the vehicle that must be taken into account during the aircraft conceptual design. Another structural area of research is examining the impact of the design safety factor on the vehicle reliability [31,32]. This challenge has the potential to be further explored through a design environment similar to the one described herein; however, this exploration is outside the scope of this paper. Finally, it has been observed that most of the mentioned structural challenges use higher-fidelity tools like CFD and finite element methods (FEM) to predict the structural behavior of the vehicle [33,34]. Lower fidelity tools based on linear elasticity theory, energy, and variational principles can also be used to determine the structures stresses and displacements.

The objectives of the proposed environment with respect to the UAV design challenges can be divided into two categories. The first objective is to take advantage of the existing disciplinary models by combining their strengths in terms of computational time and accuracy into a single environment. The second objective is to demonstrate how the proposed environment can be used to better explore the UAV design space by allowing the analysis of a larger number of vehicle architectures.

[¶]Data available online at http://web.mit.edu/drela/Public/web/avl/, [retrieved Jan. 2008].

III. Design Background and Design Environment

The UAV conceptual design environment is part of an overarching design process. A design process, at the highest level of abstraction, represents a series of events consisting of information gathering and decision making. The role of the design environment is to enable good decision making by compiling good information.

One objective of this research is to create a design environment that integrates requirements analysis and conceptual design of a new vehicle. The steps listed in Fig. 1 describe specific tasks that must be performed during the UAV design process; they are taken as reference from the International Council on Systems Engineering (INCOSE) handbook [35]. The first step is to define the systems goals and objectives of the project; an example of the application of the goals, objectives, technical challenges, and applications (GOTChA) charts can be found in [36]. The modeling and simulation in step 6 corresponds to the UAV design environment, which has the overarching goal of verifying that the different systems alternatives meet the objectives and requirements specified by the customers.

Furthermore, the modeling and simulation environment (Fig. 1, step 6) provide a quantitative assessment of the vehicle performance and a means to perform uncertainty analysis. Uncertainty analysis is another important challenge of conceptual design because of the large design freedom and incomplete knowledge of the system. The design environment can be used to propagate the uncertainty in the system and to assess the impact of the uncertainty on the final vehicle configuration [37]. The next subsections describe the variable fidelity attribute and the construction of the design environment.

A. Variable Fidelity Attribute

In a publication on "Decision Support Methods and Tools," it is emphasized that future design environments should be flexible, variable fidelity, robust, and validated [38]. Flexibility and variable fidelity are the main objectives in the development of the proposed design environment. The flexibility attribute was discussed in the preceding section, whereas this section discusses the variable fidelity attribute of the design environment.

The level of fidelity can be defined as how well a mathematical model represents the actual physical behavior. For instance, modeling the airflow over a wing can be done using lifting line theory, vortex lattice theory, Navier–Stokes equations, or wind-tunnel experimentation. Assuming that a wind-tunnel experiment captures the true physical behavior of the flow, the various analytical results can be compared with the physical results to determine their modeling error. Practically, the level of fidelity is correlated with the computational time required to obtain the results, assuming that more accurate models are more computationally expensive. In this paper, the levels of fidelity have been divided by orders of magnitude of computational time: low fidelity implies that results can be obtained in seconds, medium fidelity implies minutes, and high fidelity implies hours or days.

The variable fidelity philosophy is derived from the doctrine of successive refinement illustrated in Fig. 2 and further discussed in the NASA Systems Engineering Handbook [39].

The doctrine of successive refinement starts with a set of needs, capabilities, or opportunities in the field of study. Generally, a large amount of information is required to adequately define the problem because the level of knowledge about the new vehicle is limited while the uncertainty is large. The objective is to reduce the uncertainty while increasing the knowledge about the system. This is achieved by exploring the design space, and by increasing the level of fidelity of the analysis tools. Consequently, the process starts with lower fidelity tools enabling a larger exploration of the design space because of their reduced computational time. The next section presents how the UAV design environment is built with the flexibility and variable fidelity attributes in mind.

B. Unmanned Aerial Vehicle Conceptual Design Environment

A key characteristic of a design environment is its ability to perform the vehicle sizing and synthesis. The initial characteristics of a new system are defined from the customer requirements. The sizing process then scales the physical dimensions of the systems, whereas the synthesis process uses these dimensions in the disciplinary tools to calculate the vehicle's performance. The process iterates between the sizing and synthesis until the requirements are matched in terms of power, energy, and geometric dimensions [40]. This section describes how the synthesis and sizing processes are implemented in the creation of the new design environment.

The synthesis process starts by combining the disciplinary tools in an integrated framework. The integrated framework facilitates the communication among the various disciplinary models. There are a number of software packages commercially available that can achieve this task. Phoenix Integration's ModelCenter® was selected to be the integrating design framework because of its flexibility, modularity, ease of use, and previous experience in using it by the authors.

ModelCenter allows the behavior of the overall environment to be controlled using a series of scripts that define the sequence of

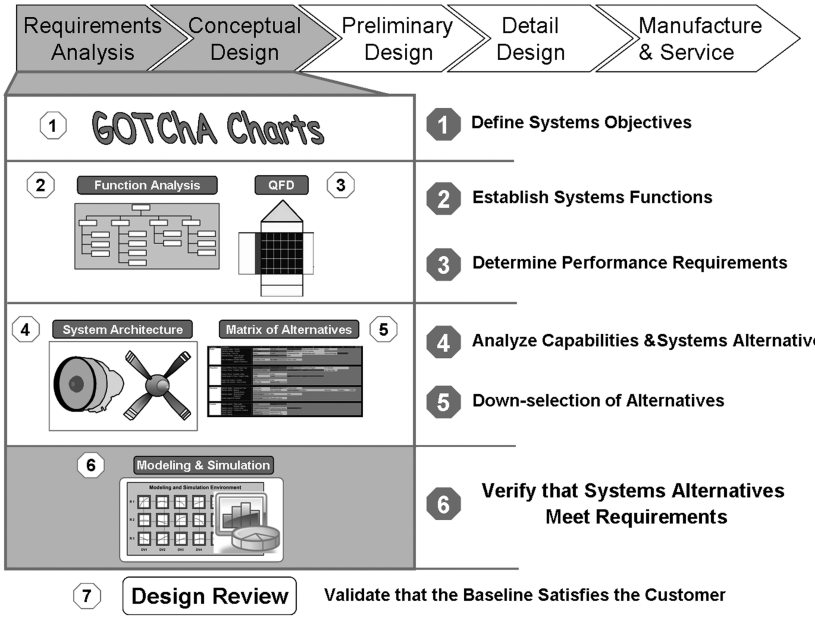

Fig. 1 Systems engineering design process (steps from [35]).

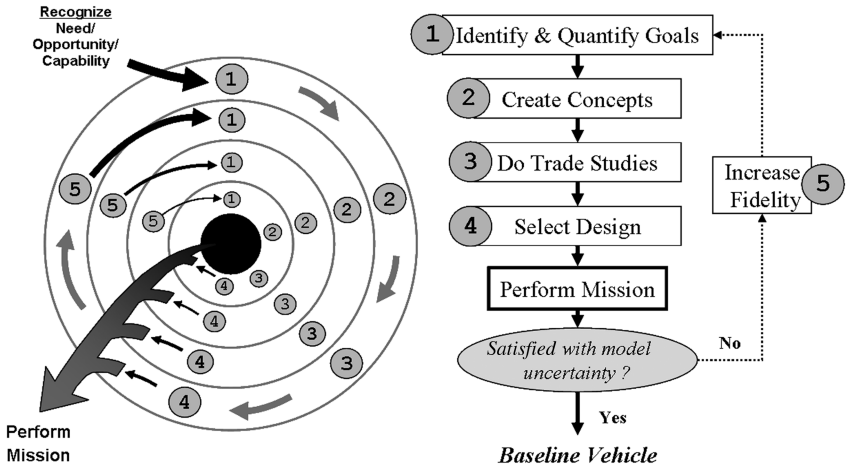

Fig. 2 Doctrine of successive refinement (modified from [39]).

analyses and control the flow of data.[**] Scripts are also used for each disciplinary analysis tool to translate the variables from the environment into the parameters required as inputs to the tools as well as to translate the outputs of the tools into the terms required by the overall environment.[††] Multiple models with different levels of fidelity can be integrated for each discipline into the common framework. This variable fidelity capability enables the user to balance the complexity of the analysis against the required run time by selecting which level of fidelity is appropriate for each discipline. Table 1 lists the different disciplinary tools implemented in the design environment.

The implementation of these disciplinary tools in the ModelCenter environment is shown in Fig. 3. The main inputs of the environment include a baseline geometry, an operational mission, the design flight conditions, and the preferred sizing strategy. The design flight condition and sizing strategy are discussed later in this section.

Once the inputs are defined, the user selects the desired airfoil analysis tool to evaluate the aerodynamic coefficients (Fig. 3, step 1). The user has the choice between PABLO,[‡‡] XFOIL [42], or experimental data, if they are available. PABLO is relatively fast and accurate for inviscid flow, whereas XFOIL is fast and accurate for both inviscid and viscous flow. Multiple airfoil analyses can be performed, and the results are stored in text files accessible to the aerodynamics and structural modules.

The second step shown in Fig. 3 is to model the geometric variables in a computer-assisted design (CAD) software. The CAD tool used in the environment is the NASA-developed vehicle sketch pad (VSP), which is an extension of the rapid aircraft modeler (RAM) [43]. This tool includes a set of predefined aircraft parameters for wings, fuselages, and pods and also calculates the wetted area of the individual geometric elements for friction drag calculations. Using the baseline geometry, VSP computes lift, induced drag, and aerodynamic moments through a vortex lattice solver called VORLAX [23] (Fig. 3, step 3). It should be noted that other lift sources, like buoyancy and thermal lift, are outside the scope of the current study.

Analyzing a complex geometry in VORLAX can be time consuming. For that reason, a numerical lifting line code [20] was added to the aerodynamics module to compute the lift and induced drag of a simple wing design. The drag breakdown is completed with the evaluation of friction drag using either airfoil data or form factor empirical relationships.[§§] The form factor code is based on empirical equations that are a function of the Reynolds number and the wetted area of the individual components. The airfoil approach requires the numerical integration of the airfoil sectional drag over the lifting surface. This technique has been coded in MATLAB® and requires the use of the airfoil analysis results previously calculated. The vehicle aerodynamics coefficients are also stored in a text file that is used during the mission simulation (step 6).

Once the aerodynamic characteristics of the vehicle are computed, the information is transferred to the structures module to evaluate the deflected geometry (Fig. 3, step 4). The structures module calculates the wing deflections, wing weight, and root stresses based on an equivalent beam having predefined cross-sectional properties. The cross-sectional properties are obtained using variational asymptotical beam sectional analysis [44] (VABS©).[¶¶] The properties are then used as inputs to DYMORE©, which performs a structural analysis of the equivalent beam giving the wing deflections and root stresses.[***] The actual weights calculation can be performed by summing the resulting structural masses or from empirical wing data [45,46]. The option is then provided to iterate back with the structurally deflected geometry to update the geometry model and reevaluate the aerodynamic characteristics.

The propulsion module, Fig. 3, step 5, includes six propulsion architectures combining power systems, propulsive systems, and power management and distribution (PMAD) systems. The propulsion architectures are listed in Table 2. Each has a fuel source (either hydrogen or a battery) and an oxidizer source (either an oxygen tank or air from the atmosphere of an air compressor for high altitude flight), with the exception of the battery, which has no need for an oxidizer. The propulsive system is identical for all architectures; it includes electrical motors with gearbox and propeller models. The propulsion architectures are modeled in MATLAB Simulink® and integrated into the ModelCenter environment. The selection of the desired propulsion architecture is an input to the design environment. The modularity of the environment enables tradeoffs between the different propulsion systems because the architectures have a common set of inputs/outputs. The lower fidelity option for the propulsion module includes the engine decks stored during a previous sizing iteration. However, this option is limited because the performance of most architecture depends on the operational time and location of the vehicle. For instance, the power output of the solar panels depends on the orientation of the vehicle relative to the sun, which is a function of the time of day at that location and the flight direction.

In addition to the stored drag polar and the selection of the propulsion architecture, the propulsion system needs to be sized to

[**]Data available online at http://www.phoenix-int.com/~AnalysisServer/ScriptWrapper/index.html [retrieved Jan. 2008].

[††]Data available online at http://www.phoenix-int.com/~AnalysisServer/FileWrapper/index.html [retrieved Jan. 2008].

[‡‡]Data available online at http://www.nada.kth.se/~chris/pablo/pablo.html [retrieved July 2007].

[§§]Data available online at http://www.aoe.vt.edu/ ~mason/Mason_f/MRsoft.html [retrieved April 2007].

[¶¶]Data available online at http://www.mae.usu.edu/faculty/wenbin/ht_docs/vabs.html [retrieved 5 July 2007].

[***]Data available online at http://www.ae.gatech.edu/people/obauchau/ [retrieved 30 May 2007].

Table 1 Variable fidelity analysis tools considered in design environment (inspired by [41])

		Discipline					
		Geometry	Airfoil	Aerodynamics: friction drag	Aerodynamics: lift and induced drag	Structures	Propulsion
Fidelity	Low	2-D model[a]	Inviscid (PABLO)[b]	Empirical method (form factor)[b]	Lifting line[b]	Regressed equations[b]	Table lookup[b]
	Medium	Vehicle sketch pad (VSP): 3-D[b]	Inviscid–viscous (XFOIL$^{(GNU)}$)[b]	Airfoil numerical integration[b]	Vortex lattice (VORLAX)[b]	Finite element (DYMORE)[b]	Matlab/Simulink modules[b]
	High	CATIA V5®[a]	Experimental data[b]	CFD–Fluent®	CFD–Fluent[a]	FEM-ANSIS®[a]	Experimental engine data[a]
	High	offline	——	CFD–Fluent[a]	——	CFD_Fluent[a]	FEM-ANSIS[a]
——							

[a]Not implemented.
[b]Implemented.

perform the mission simulation (Fig. 3, step 6). The mission simulation is part of the sizing process discussed in the next section.

C. Sizing Process

The environment allows for both sizing to a set of requirements and analyzing off-design missions. The environment also enables simulation-based design by flying through given missions, even during the sizing iteration. Simulating the mission, rather than relying upon empirical relationships, is an important ability for an environment created to handle unconventionally powered vehicles. The sizing methodology implemented into the environment can be broken into three main components: initial propulsion sizing, mission simulation, and resizing.

The propulsion system is sized based on the power required at a design flight condition and is defined by a Mach number, altitude, and rate of climb. The power required is calculated based on the vehicle drag at that flight condition; this information is extracted from the stored drag polar calculated by the aerodynamic module. Once the propulsion architecture is sized, the propulsion mass is updated in the mass breakdown; if the new total mass is significantly different than the initial guess, the propulsion sizing iterates until convergence.

Following the initial propulsion sizing of the vehicle, the environment simulates the design mission. The mission analysis module calls the aerodynamic lookup table created during sizing and uses a full propulsion analysis at each time step. As mentioned earlier, there is also an option for a table lookup to be created from the propulsion analysis that can be reused for different missions.

The variables that describe the current state of the vehicle are updated using a first-order forward Euler method. The accuracy of the integration is aided by the fact that each simulation time step is divided into many time steps when calculating the propulsion properties. Consequently, the overall accuracy is greater than it would be using the regular Euler method.

Several sizing checks are performed at every simulation time step. These checks verify that the vehicle has sufficient lift, power, or fuel at every point of the mission analysis. If one of these checks fails, then the environment will automatically resize the vehicle. The resized vehicle will then start the process over at the very beginning with the initial values modified to avoid violating the same constraint.

The current sizing process depends on a single design point, cruise conditions, and the design mission. This is clearly not adequate to capture all the performance requirements of a prospective vehicle. To accomplish this, it is desired to integrate a constraint analysis into the design environment [47]. The constraint analysis could be used to populate the initial scale for the sizing variables at the beginning of the design process, as well as to ensure that the final vehicle meets the full set of performance requirements. This part of the design environment has not been currently implemented and remains for future work.

IV. Application of Design Environment

The integration of the disciplines within the ModelCenter environment required a significant amount of time to ensure the traceability of the variables among the different modules. Each disciplinary module of the environment was validated separately. The verification of the overall environment was performed by modeling the Pathfinder Plus platform as shown in Fig. 4. The first part of this section presents a comparison of the design results with publicly available data, whereas the second part presents specific performance results obtained from the design environment.

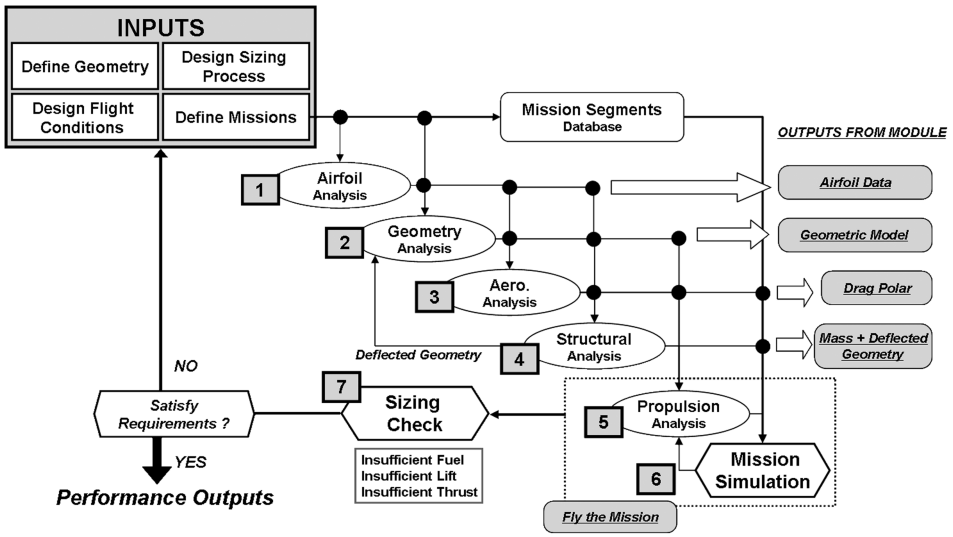

Fig. 3 Design structure matrix of conceptual environment.

Table 2 Propulsion architectures

	Power systems	PMAD
1	Solar cell and fuel cell	Electrolyzer, H_2 tank, O_2 tank, and H_2O tank
2	Fuel cell	H_2 tank and O_2 tank
3	Solar cell and fuel cell	H_2 tank and O_2 tank
4	Solar cell and fuel cell	H_2 tank and centrifugal air compressor
5	Solar cell	Rechargeable battery pack
6	Hydrogen internal combustion engine	H_2 tank and centrifugal air compressor

The design variables used to model the Pathfinder Plus are depicted in Table 3 [48]. The first step was to create the undeflected geometry as illustrated in Fig. 5a. The deflected geometry, Fig. 5b, was obtained after the first iteration between the aerodynamics and structural modules. In addition to the geometry, it is important to match the gross weight of the vehicle because of its strong influence on the mission analysis.

The assumptions used in running the validation cases are shown in Table 4. The first major assumption is the mass breakdown. The total mass and payload mass are known from available data, but the other masses had to be estimated. The structural mass was evaluated from an empirical relationship for solar-powered UAVs [46]. The battery mass was sized to match the assumed specific power of 100 W/kg at the takeoff condition; 6 kW of power was assumed to be generated from the solar cells, whereas the battery generated the remainder of the total output power. The 6 kW power assumption was verified using the environment's propulsion module. The other propulsion mass, which includes the propellers, motors, and power management system, corresponds to the difference between the other masses and the known total mass of 315 kg.

Regarding the vehicle aerodynamic assumptions, first the geometry of the vehicle is simplified. It does not include the motor nacelles, the two cylindrical external pods, and the landing gear as shown in Fig. 4. All these missing components have an impact on the skin friction drag, which will be described in the drag breakdown discussion. Second, the flow condition is assumed to be fully turbulent for the evaluation of the airfoil aerodynamics coefficients and also for the skin friction form factor model.

The objective of the structural module was not to design the internal structural layout of the wing but to provide a deflected geometry to the aerodynamic model. Consequently, the internal layout of the wing includes a graphite-epoxy circular spar with no other structural components, that is, skin or foam. The desired wing tip deflection to match the geometric deflection of the vehicle in flight, Fig. 4, is 2 m. This wing deflection corresponds to 11% of the wing semispan and was matched by varying the diameter of the spar. The current structural analysis with VABS and DYMORE has currently only been validated with a box and circular beams layout.

The first verification of the environment was done using the altitude profile of the Pathfinder Plus [49]. This mission profile was approximated in the modeling environment using the available mission segments. The comparison of the actual and modeled mission profiles is displayed in Fig. 6. The altitude profile is not exactly captured because the climb rate was not directly specified. Instead, the mission analysis uses climb segments based on specified lift coefficients and power settings, rather than Mach numbers and climb rates. The overall agreement is still quite good and demonstrates the ability of the modeled vehicle to perform the same mission as the real Pathfinder Plus. Because of the lack of publicly available data, this comparison by itself does not validate that the modeled UAV accurately duplicates specific performance characteristics of the actual Pathfinder Plus.

Fig. 4 Pathfinder Plus in flight [50].

Table 3 Pathfinder Plus inputs

	Geometry [48]
Chord, m	2.4 [8 ft]
Span, m	36.9 [121 ft]
Central section span, m	13.41 [44 ft]
Wing aspect ratio	15
Airfoil central section[a]	Selig S6078
Airfoil [49]	Liebeck LA2573A
	Mission [48]
Cruise speed low altitude, m/s	7.6–9.4 [17–21 mph]
Cruise speed at 18,300 m, m/s	28.7 [64 mph]
Power off glide ratio	21
	Propulsion [48]
Number of engines	8
Motor power, kW, each	1.5
Battery backup power, h	2–5
Total power output, kW	12.5
Solar cells efficiency, %	19
	Structures [48]
Gross weight, kg	315
Payload weight, kg	67.5
Primary materials	Carbon fiber, Nomex®, Kevlar®, plastic sheeting, and plastic foam

[a]Data available online at http://www.ae.uiuc.edu/m-selig/ads/aircraft.html [retrieved 7 July 2007].

The second verification compares the actual and predicted velocity profile of the Pathfinder Plus, as illustrated in Fig. 7 [51]. The actual velocity in Fig. 7 comes from a completely different mission than the altitude profile displayed in Fig. 6, and this explains the maximum altitude being lower in Fig. 7. The predicted profile in both instances is from the same mission; this was necessary because detailed information could not be found to completely characterize a full Pathfinder Plus mission. Furthermore, the modeled velocity profile is based on specified lift coefficients chosen during the climb rather than on climb rates. This difference is assumed to be one cause of the discrepancy between the actual and predicted data. Nevertheless, the agreement between the two curves is generally good, which indicates

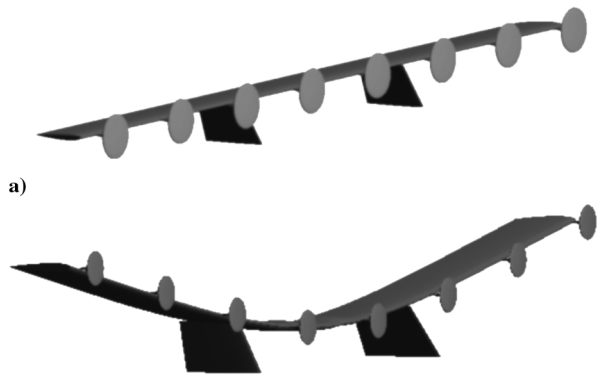

a)

b)

Fig. 5 Pathfinder Plus in VSP: a) undeflected geometry; b) deflected geometry.

Table 4 Modeled Pathfinder Plus assumptions

System	Name	Value	Units
Mass breakdown	Total mass	315	kg
	Structural mass	115.8	kg
	Payload mass	67.5	kg
	Battery mass	65	kg
	Other prop. mass	66.7	kg
Propulsion	Date	March 2003	——
	Initial latitude	25	Deg N
	Solar cell efficiency	19	%
	Total power	12.5	kW
	Batt. specific power	100	W/kg

that our atmospheric and aerodynamics models provide realistic trends and reasonable results.

Next, we will present more detailed performance results obtained from the Pathfinder Plus case study. These results illustrate some of the specific capabilities embedded in the conceptual design environment.

Because of the limited amount of publicly available data on the Pathfinder Plus performance, this section describes specific performance obtained from the Pathfinder Plus modeled in the design environment. The first performance characteristic is the vehicle flight envelope, which provides an overview of the operational capabilities of the aircraft. This section also presents the main aerodynamics and propulsion performance characteristics.

The flight envelope was generated by combining contours of specific excess power calculated from Eq. (1). In Fig. 8, the specific excess power contours are equaled to zero, corresponding to the operational limits of the vehicle.

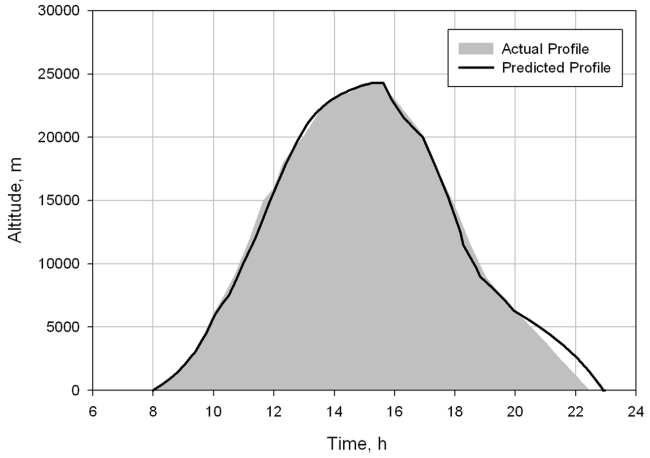

Fig. 6 Pathfinder Plus mission profile [49].

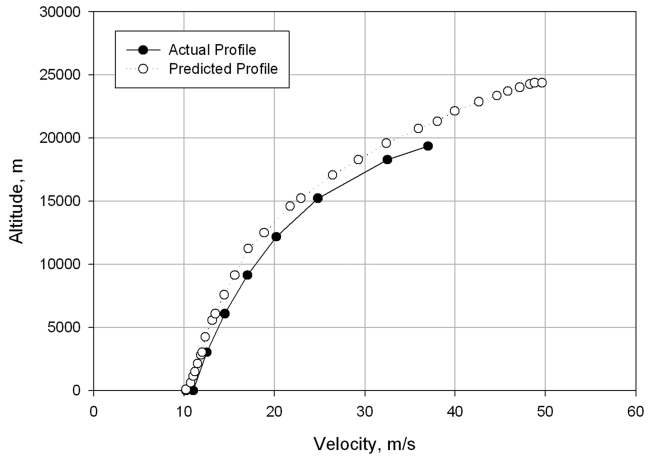

Fig. 7 Pathfinder Plus velocity profile [51].

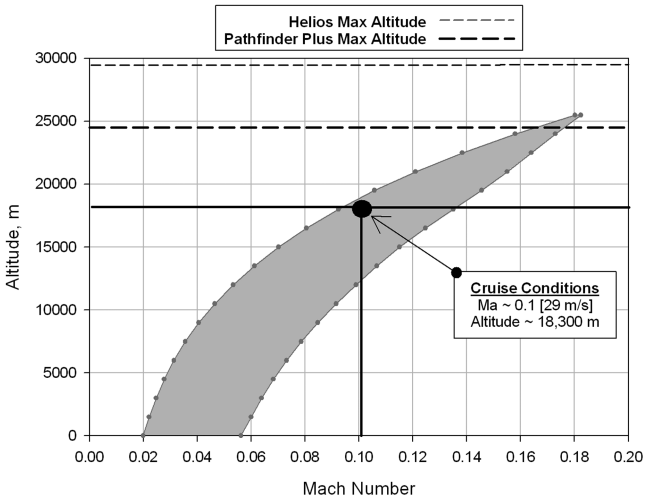

Fig. 8 Pathfinder plus flight envelope.

$$\text{specific excess power} = \frac{V(T_A - D)}{W_i} \tag{1}$$

where V is the velocity (m/s), T_A the thrust available in Newtons, D the vehicle drag in Newtons, and W_i the vehicle's weight in Newtons. The true flight envelope would not be solely a function of the aerodynamics and propulsive characteristics of the vehicle as there can be significant structural limits on the velocity, but this was not explored in this study.

The flight envelope enables the visualization of the absolute and service ceilings of the aircraft. The calculated absolute ceiling, shown in Fig. 8, is very close to the maximum altitude reach with the prototype aircraft (24,445 m) [48]. The absolute ceiling strongly depends on the propulsion architecture and the aerodynamics model. The Pathfinder Plus propulsion architecture includes electric motors, high-altitude propellers, and a backup battery system. This flight envelope demonstrates the ability of the environment to calculate reasonable aerodynamics and propulsion performance. A thorough validation of the flight envelope is harder to obtain because the only glide ratio data available is at an unspecified cruise condition. The remainder of this section will describe additional performance results of the modeled Pathfinder Plus at cruise conditions.

Based on the geometric model, the aerodynamic performance of the vehicle is evaluated by the environment. Figure 9 shows the airfoil aerodynamic coefficients obtained with XFOIL at cruise conditions. It is observed in Fig. 9a that XFOIL can estimate the maximum two-dimensional lift coefficient. The airfoil drag polar, Fig. 9b, is stored in a text file and accessed to calculate the wing friction drag.

The drag breakdown of the vehicle at cruise conditions is illustrated in Fig. 10. The main drag contributors are the induced drag, calculated by VORLAX, and the friction drag, calculated differently depending on the vehicle component. By default, the friction drag for fuselages and pods is evaluated using the form factor based empirical equations, whereas the lifting surface friction drag is evaluated by numerical integration of the airfoil aerodynamic coefficients over the wing. The friction drag of the eight motor nacelles was estimated using an approximation of their geometry as modeled in VSP combined with the form factor code, whereas the landing gear interference drag was estimated using methods from [52]. The total drag also includes the miscellaneous drag, which takes into account the interference and surface roughness drag. The value assumed for the miscellaneous drag in Fig. 10 was selected to match the estimated power-off glide ratio of the actual Pathfinder Plus from [48]. There is some uncertainty surrounding this glide ratio value as [48] does not specify the flight condition for this value, or even if the glide ratio is a calculated or experimental result. This might explain the relatively large miscellaneous drag component. Additionally,

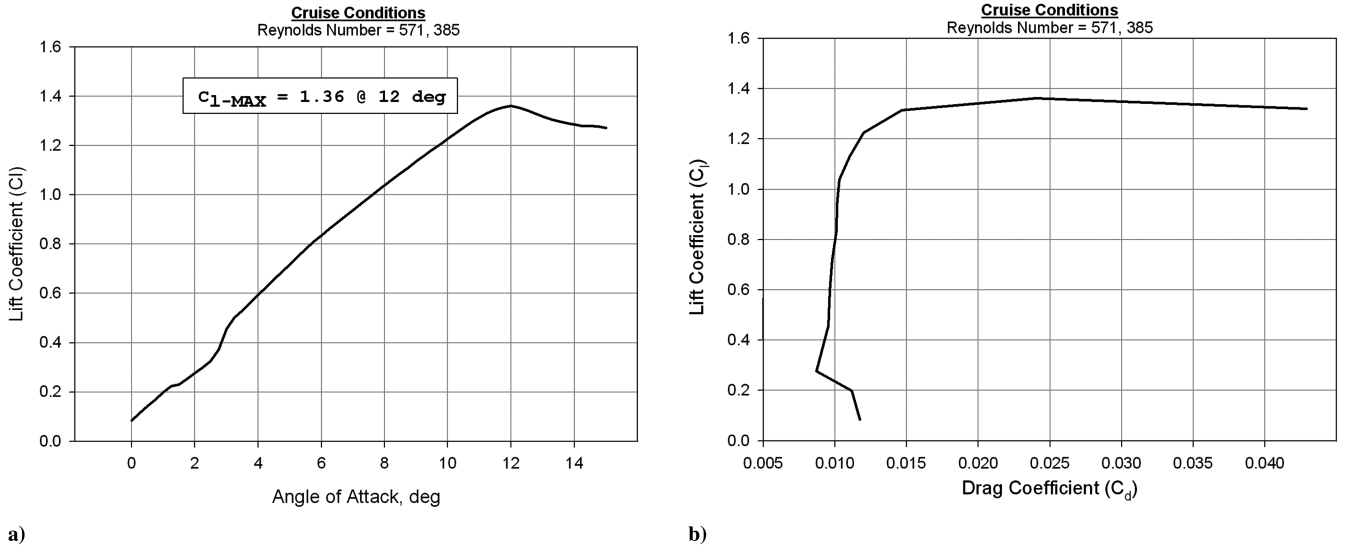

a) b)

Fig. 9 Airfoil (Liebeck LA2573A) analysis at cruising conditions.

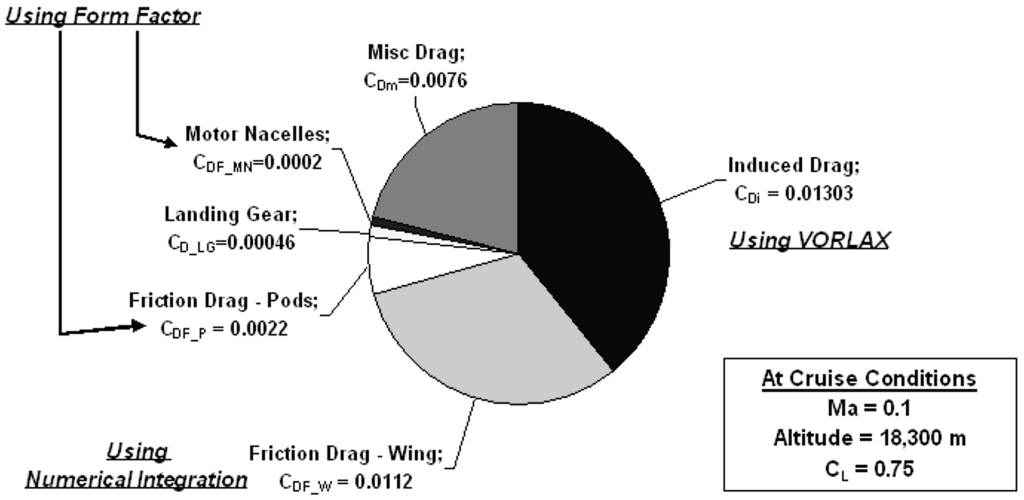

Fig. 10 Drag coefficients breakdown.

some pictures of the Pathfinder Plus include seven wing-mounted turbulence instruments [53] that were not included in the drag estimation. The potential error in the drag estimation is a good example for the need to increase the level of fidelity following the design space exploration. Combining the total drag with the lift coefficients, obtained from VORLAX, results in the drag polar shown in Fig. 11. The drag polar is then stored in a text file so that it can be rapidly called during mission analysis.

The propulsive performance of the vehicle is calculated in three main stages. The first stage is a semi-empirical evaluation of the battery discharge over each time step. The second stage evaluates the solar power available based on the date, time of day, altitude, wing area, solar cell efficiency, the percentage of the wing that is covered with solar cells, and the orientation of the vehicle relative to the sun. The final stage evaluates the thrust through calculation of the propeller efficiency at the given flight condition. The net result is that the battery state of charge and the thrust available are calculated for each time step. The thrust available and thrust required are displayed in Fig. 12. The intersection of the thrust available and the thrust required for a given altitude is what defines the maximum velocity in Fig. 8.

The structural module of the environment includes a cross-sectional analysis of the airfoil with VABS, and the structural analysis of the wing with DYMORE. The current version of the structures module is not yet mature enough to parametrically analyze a cross section as complex as the one used by the Pathfinder Plus. The cross section represented in Fig. 13 includes a nonstructural skin combined with a circular spar. The structural module can estimate the wing bending and the stress distribution at the wing root based on the beam definition and the aerodynamic loading at cruise conditions. The wing deflection shown in Fig. 14 was obtained with a circular spar 16 cm in diameter and with 0.5 cm of wall thickness. It should be

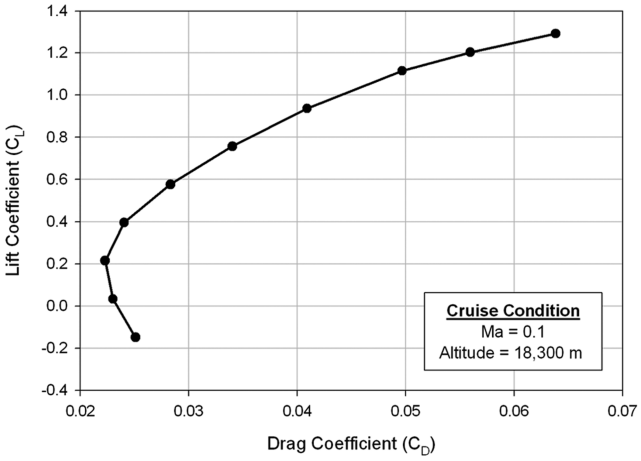

Fig. 11 Pathfinder Plus drag polar at cruise conditions.

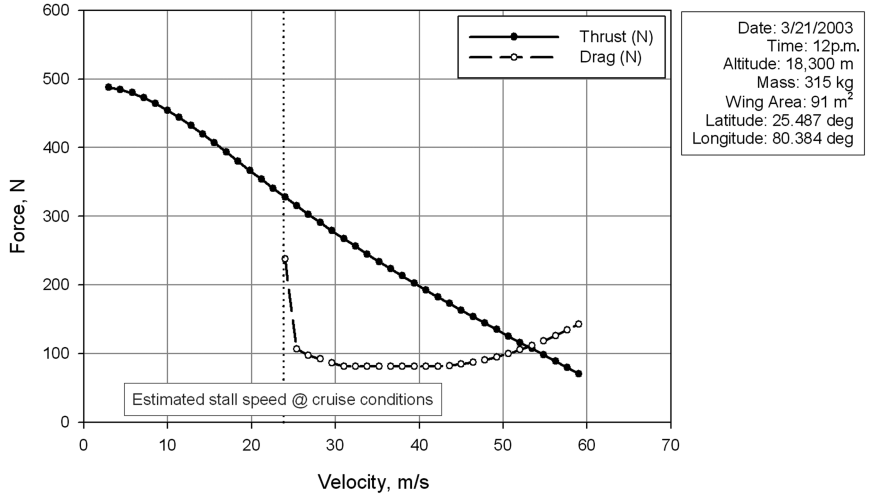

Fig. 12 Pathfinder Plus thrust curves at cruise altitude.

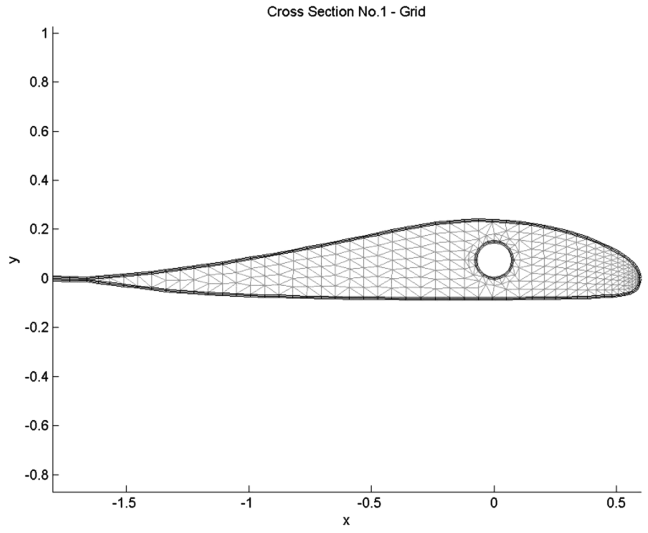

Fig. 13 Cross-sectional grid of airfoil Liebeck LA2573A.

noted that with the current state of the design environment, only an approximation of the wing deflection was required to update the vehicle aerodynamics characteristics. The estimation of the structural mass from the structural module is left for future work, with current mass estimates coming from empirical relationships.

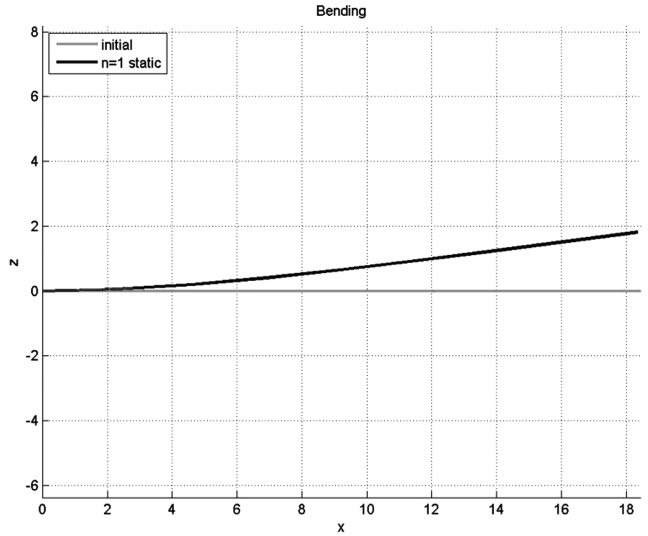

Fig. 14 Wing deflection from DYMORE (axis in meters).

V. Case Study: Hurricane Tracker

One of the objectives for creating the UAV conceptual design environment is to explore the ability of an existing vehicle to perform a new type of mission. By doing so, the design team can gain valuable information about the different systems and technologies required to successfully execute the mission. This section explores the capability of the Pathfinder Plus aircraft to perform a hurricane-tracking mission. The main goal of the case study is to demonstrate the ability of the UAV conceptual design environment to explore the mission design space. Secondary objectives are to identify design tradeoffs and to identify the technology enablers.

The notional hurricane-tracking mission states that the aircraft platform should take off from the coast of Florida, fly to Cape Verde (western coast of Africa), loiter on station until the formation of a tropical storm, and follow the formation of the tropical storm into a hurricane while gathering data on the storm system. This mission has been constructed from segments listed in Table 5 and illustrated in Fig. 15. The total mission time works out to approximately eight days.

The primary technical challenge for the aircraft is to stay in the air for the entire mission. The main technology enabler in this case is the propulsion architecture. The baseline propulsion architecture of the Pathfinder Plus as modeled in the environment includes solar cells and rechargeable batteries. Therefore, the objective is to find the combination of solar cell efficiency and battery specific energy that will allow the vehicle to fly the entire mission without landing. To explore this issue, the modeled Pathfinder Plus was set to fly a climb and loiter mission to test the endurance for a range of battery specific energy and solar cell efficiency values. The solar cell efficiency is based on a semiphysical and semi-empirical model of solar radiation [54]. The results of this analysis are presented in Fig. 16.

The test mission used to create Fig. 16 starts at 8 a.m. local time (March 2003, lat 25°N), and, assuming a constant battery mass, no combination of solar cell efficiency and battery specific energy resulted in a vehicle capable of flying through a single night. The effect of solar cell efficiency clearly diminishes beyond 25%, whereas the battery specific energy has a continuously large impact on the performance. As reference, the solar panel efficiency of the actual Pathfinder Plus was around 19%, whereas today's commercially available solar panel efficiency are around 21.5%,[†††] and solar panels used for space missions can reach 26.7% [55]. Furthermore, current lithium-ion battery modules have specific energies around 150 $W \cdot h/kg$ [56,57]. These results suggest that

[†††]Data available online at http://www.sunpowercorp.com/homeowners/panels.html [retrieved 4 Aug. 2007].

Table 5 Hurricane-tracking mission

	Mission segment	Climb rate, m/s	Power setting, %	Final altitude, m
1	Takeoff	0.45	95	100
	Mission segment	Lift coefficient	Power setting, %	Final altitude, m
2	Climb	1.1	95	19,812
	Mission segment	Lift coefficient	Range, km	Mach number
3	Cruise	0.75	5783	0.11
	Mission segment	Lift coefficient	Time on station, h	Turn load factor
4	Loiter	1.1	73	1.05
	Mission segment	Lift coefficient	Range, km	Mach number
5	Cruise	0.75	3453	0.11
6	Cruise	0.75	2248	0.11
7	Cruise	0.75	1736	0.11

even with massive technological improvements, it is not currently feasible to achieve a regenerative battery system with the modeled Pathfinder Plus.

The decision was made to explore a change in propulsion architecture to a rechargeable hydrogen fuel cell system. A brief look at various combinations of hydrogen mass and solar cell efficiency, with other variables set to nominal values, suggested that it might be possible to achieve a regenerative vehicle by using a fuel cell architecture. The next step was to perform a design space exploration to determine what combination of variables would allow the system to be regenerative, and therefore capable of performing the hurricane-tracker mission.

A. Exploration of Vehicle Design Space

The construction of a conceptual design environment is a not an end unto itself; rather, it is the means to the end of making better and more informed design decisions. In conjunction with a design environment, surrogate models are a useful tool in enabling the full range of design options to be explored. A surrogate model is an approximation of a more complicated analysis tool or, as in this case, suite of analysis tools with a representation limited to a specific problem. Surrogate models, also known as meta models, are an enabling technique for a range of advanced design methods that enable more informed and better design decision making [58]; some of these advanced techniques will be applied using the present environment to demonstrate their potential benefit. The analyses presented herein are intended only to be representative and not encompass all possibilities.

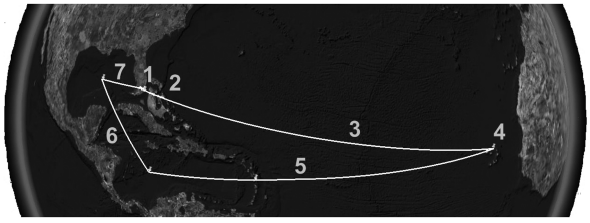

Fig. 15 Hurricane-tracking mission plotted in Google Earth™.

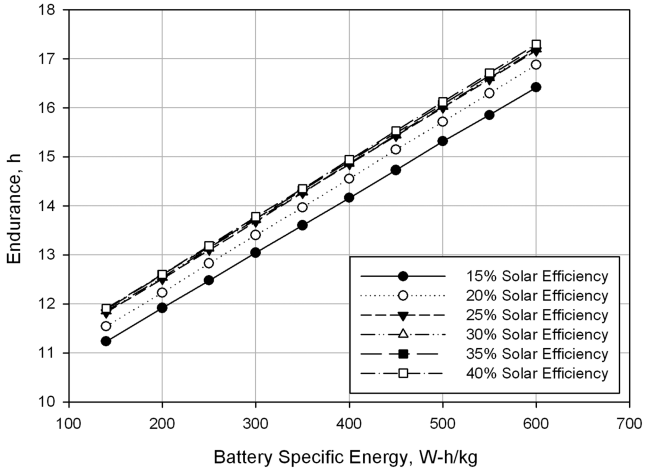

Fig. 16 Analysis of the impact of solar cell efficiency and specific energy on mission endurance.

Response surface methodology (RSM) was used to create the surrogate models. This approach uses a polynomial model, typically second order, with the specific design variable combinations required to create the model based on design of experiments (DoE) methods. The form of the equation for a second-order model can be seen in Eq. (2), where R is the response being modeled, the xs are the design variables, and the β values are coefficients of the polynomial. The whole process has been automated in the commercially available JMP® statistical software suite.

$$R = \beta_o + \sum_{i=1}^{k} \beta_i x_i + \sum_{i=1}^{k} \beta_{ii} x_i^2 + \sum_{i=1}^{k-1} \sum_{j=i+1}^{k} \beta_{ij} x_i x_j \tag{2}$$

The first step in creating a surrogate model is determining which responses are important and which design variables most affect the response values. Four different responses were chosen as important metrics for this study: total vehicle mass, round-trip efficiency, percent regenerative (P_{regen}), and system specific energy. The last three responses are depicted in Eqs. (3–5):

$$\text{round-trip efficiency} = \bar{E}_{\text{fc}}/\bar{E}_{\text{ez}} \tag{3}$$

$$\text{percent regenerative} = (E_{\text{solar}} + E_{\text{ez}}\eta_{\text{ez}})/E_{\text{total}} \tag{4}$$

$$\text{specific energy} = E_{\text{fc}}/m_{\text{prop}}n_{\text{days}} \tag{5}$$

The round-trip efficiency measures the ratio of the energy produced by the fuel cell per kilogram of hydrogen ($\bar{E}_{\text{fc}}$) over the energy consumed by the electrolyzer per kilogram of hydrogen ($\bar{E}_{\text{ez}}$). The percent regenerative equation evaluates the energy consumed from the power sources ($E_{\text{solar}}, E_{\text{ez}}$) over the total energy consumed to power the vehicle (E_{total}). The specific energy equation is defined as the total energy produced by the fuel cell over the propulsion system mass times the number of days flown by the vehicle.

The previous definitions are not always conventional. The round-trip efficiency is commonly defined only for a closed regenerative system [59]. During the design space exploration, not every combination of variables resulted in a regenerative system. Consequently, the alternate definition of Eq. (3) was used, because it provides a reasonable estimate of the efficiency even for systems that are not fully regenerative. The percent regenerative metric attempts to capture how regenerative the system is; values greater than one indicate that the energy input from the sun more than equals the energy required to fly the mission and the vehicle should therefore be fully regenerative. The system specific energy is a metric capturing the energy storing capacity of the system. For a regenerative system, the specific energy is directly proportional to the length of time considered, because it is constantly storing more energy while the

Table 6 Design space exploration variable summary

Number	Variable	Description	Baseline	Min	Max	Units
1	S	Wing area	91	60	120	m^2
2	AR	Aspect ratio	15	12	20	——
3	$kgH2$	Amount of hydrogen carried	3.5	3	5	——
4	$Wpld$	Payload weight	67.5	0	100	kg
5	Kv	Voltage constant	1	50	200	RPM/V
6	fcV	Single fuel cell design output voltage	0.7	0.5	0.8	V
7	ezV	Electrolyzer voltage	1.8	1.7	2.1	V
8	$sa\ eff$	Solar cell efficiency	0.16	0.2	0.5	——

electrolyzer is working. Therefore, it was decided to normalize the specific energy by the number of days flown, because regenerative fuel cell specific energies quoted in the literature were defined over a 24 h period [60].

A list of potentially important design variables was compiled, and a screening test was performed to determine their relative performance in capturing the variability of the responses. The details of the screening test are omitted in this paper. The result was that eight variables were the most important, and they were chosen to explore the design. The eight variables are listed in Table 6, along with a description and the ranges over which they are allowed to vary. It should be noted that the payload mass is allowed to go down to zero; this would correspond to a technology demonstrator without a useful payload.

An 81-case face-centered central composite design of experiments was created to determine what combinations of the eight variables to run. An additional 40 randomly chosen points were used to validate the surrogate models. The full 121 cases were run through the design environment, and after each case the relevant responses were stored in a file. At the end of the process, surrogate models of the responses were created based on the performance results and the DoE. The resulting models' validity was tested, with all of the responses capturing 99% or more of the variability of the responses, except for round-trip efficiency, which was at 97%. This was deemed acceptable, as the focus of the study was not on capturing the round-trip efficiency.

A sensitivity analysis of the resulting surrogate models can be seen in Fig. 17. The profile lines display the sensitivity of each of the responses to each of the input variables. The current variables values are from an unconstrained optimization that was performed to maximize the percent regenerative, with smaller weightings applied to minimize the mass, maximize the specific energy, and maximize round-trip efficiency. The payload mass was fixed to its baseline value (67.5 kg) to avoid being driven to zero. Most variables are driven to their maximum or minimum values, except for the fuel cell and electrolyzer voltages, which appear to have optimum operating conditions. The figure shows that the mass depends most strongly on wing area, payload weight, and electrolyzer voltage, whereas solar cell efficiency has no effect. The variables with the largest effect on the ability of the vehicle to be regenerative are the wing area and solar cell efficiency. The figure suggests that both a large wing area and high solar cell efficiency are required to make the vehicle regenerative. The latter of these would require a major technological advance to make a regenerative fuel cell vehicle feasible.

Some of the trends in Fig. 17 may seem counterintuitive; for example, both wing area and solar cell efficiency are positively correlated with percent regenerative but negatively correlated with specific energy. This result is due to the definition of specific energy as depicted in Eq. (5). Increasing wing area and solar cell efficiency augment the solar cell power available during the mission, which increases the percent regenerative of the vehicle as shown in Eq. (4). The additional solar cell power available then decreases the fuel cell power usage, as the vehicle is able to run solely on solar cell power for more of the mission. This reduction in fuel cell usage decreases the system specific energy, because specific energy is defined as the fuel cell energy usage divided by the propulsion system mass.

A contour plot of wing area versus solar cell efficiency is shown in Fig. 18, with the other design variables set at their baseline values. The following constraints were placed on the results from the environment: round-trip efficiency of at least 0.48, mass of at most 350 kg, percent regenerative greater than 0.9, and specific energy of at least 750 $W \cdot h/kg$. The shaded areas in the plot are regions where the design violates at least one of these constraints. The small white area shows the combinations of solar cell efficiency and wing area that simultaneously meet all of these constraints.

The nearly instantaneous function evaluations allowed by surrogate models makes it possible to perform Monte Carlo simulations, which are useful in uncertainty analysis and robust design [61]. In this paper, Monte Carlo simulations are used to explore the design space. To do that, each design variable was defined as a uniform distribution across its entire range, which was

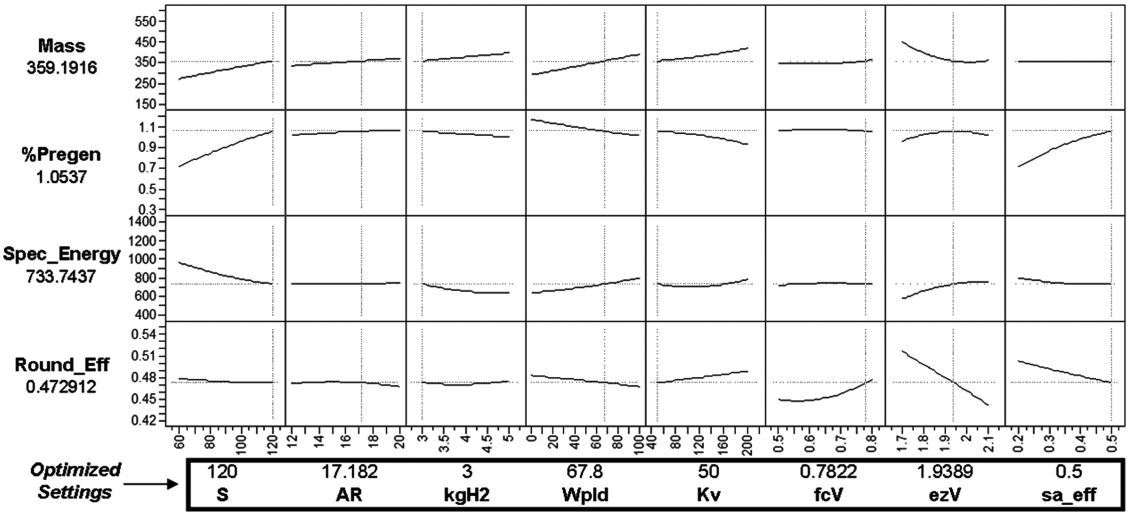

Fig. 17 Optimized design space sensitivity analysis.

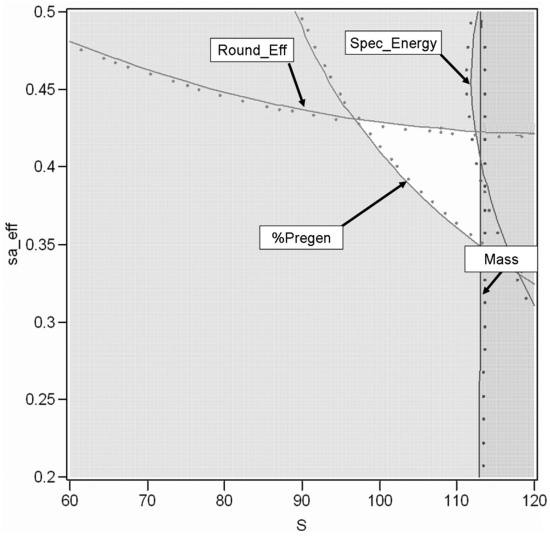

Contour Profiler

Horiz	Vert	Factor	Current X
⊙	○	S	120
○	○	AR	17.182223
○	○	kgH2	3
○	○	Wpld	67.8
○	○	Kv	50
○	○	fcV	0.7822
○	○	ezV	1.9389
○	⊙	sa_eff	0.5

Response	Contour	Current Y	Lo Limit	Hi Limit
Mass	350	359.19158	.	350
%Pregen	0.9	1.0537637	0.9	.
Spec_Energy	750	733.7437	750	.
Round_Eff	0.48	0.4729117	0.48	.

Fig. 18 Design space contour plot.

used to define a Monte Carlo simulation of 10,000 cases. This simulation took less than a second using the surrogate models, but would have taken about 19 h using the full environment.

A multivariate correlation analysis of the results is shown in Fig. 19; this figure displays the probability density functions for each of the responses, as well as pairwise comparisons of each of the responses with their correlations. From this figure, it can be observed that there is a strong inverse relationship between how regenerative the vehicle is and the specific energy of the system. The multivariate correlation analysis can also be useful in identifying how much of the design space satisfies a set of simultaneous constraints. A constraint of percent regenerative being greater than one was placed on the vehicle, and the gray points are the combinations that satisfy the constraint. Only 135 of the 10,000 cases (1.35%) meet the requirement.

All of the previously described techniques increase the knowledge of the design space, therefore enabling better design decisions. The combination of a variable fidelity design environment and surrogate models allows the designer to tailor the results for each particular system by maximizing the designer's information while minimizing the required computational time. The ability to tailor the exploration of the design space is even more important for revolutionary systems, as the initial understanding of the system is inherently going to be less than for an evolutionary system.

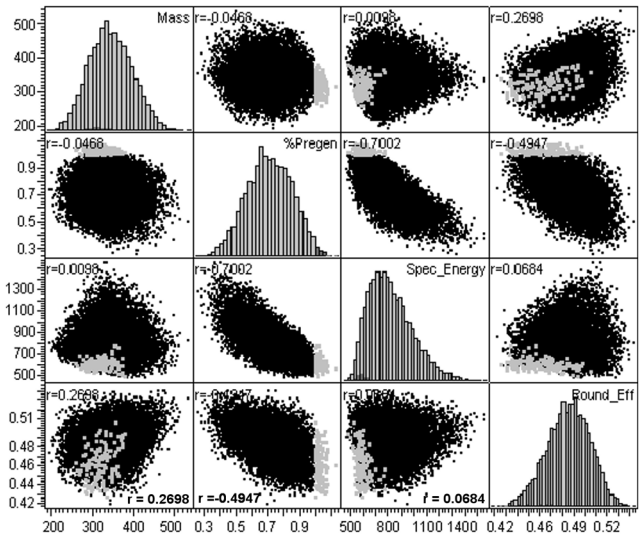

Fig. 19 Multivariate correlation analysis.

B. Results of Hurricane Tracker

Based on the knowledge acquired during the design space exploration, the values of the design variables were fixed at their optimized settings as shown in Fig. 17, with the exception of the amount of hydrogen, which was increased by 1 kg. The hurricane-tracking mission presented in Table 5 was executed using the design environment, and the results were compared with the surrogate models from the loiter mission. The results of this analysis are listed in Table 7.

The percent regenerative is not as well captured due to the inherent variation of the solar energy over the course of a significantly different mission profile for the hurricane-tracking mission relative to the simple profile used to create the surrogate models. This variation can be visualized by looking at the fluctuation of the hydrogen mass during the mission, Fig. 20. The minima in the amount of hydrogen are at different levels each day due to three factors. The first factor is related to the change in the vehicle's location on the Earth, and the change in available solar energy that entails over the course of the mission. The second factor is due to the difference in power required over the course of a different mission, because the surrogate models were created using the loiter mission. The third factor is numerical integration inaccuracies introduced over the course of the simulation; this was not explicitly measured, but could contribute to the noise. The surrogate models still provide reasonable estimates of the responses and enabled the selection of a design that was fully regenerative.

The main objective of the notional hurricane tracker was to demonstrate the design environment's ability to model a revolutionary vehicle and to fly a new type of mission. The Pathfinder Plus was used as the baseline configuration for the design space exploration; however, a real conceptual design project would have allowed more design freedom in the vehicle configuration. A more open analysis of alternatives would have expanded the number and ranges of design variables. In the context of selecting a final design configuration, the UAV design environment helps to quantify the measures of effectiveness and performance of the requirements. This information is essential for the decision makers, when the time comes to decide to pursue or to stop the development of a new vehicle.

VI. Conclusions

Currently unmanned aerial vehicles are becoming more attractive to perform missions of long duration or involving a high level of risk. This expansion of the market opens the path for the design of vehicles able to perform a large spectrum of missions, from small-range, low-altitude reconnaissance to space exploration. The ability to perform multiple missions combined with the revolutionary nature of the

Table 7 Hurricane-tracker results

Response	Design environment	Surrogate model	Units	% difference
Mass	383.1	377.8	kg	1.40
Percent regen.	1.26	1.03	——	18.39
Round-trip eff.	0.46	0.47	——	−1.84
Specific energy	606.7	655.8	W · h/kg	−8.10

systems creates uncertainty in the aircraft design. This uncertainty can only be reduced by gathering relevant information about the system. This information can then be communicated to the decision makers for the final selection of the system architecture. This research provides a means to gather important information about UAV design with the use of a variable fidelity conceptual design environment.

Variable fidelity, modularity, and flexibility are the key characteristics of the design environment. By varying the level of fidelity of the analysis tools, the design team is able to more efficiently explore the design space. Low fidelity tools are useful for the rapid survey of the design space, whereas high fidelity tools are used to converge toward a final system architecture. The modularity of the analysis tools is essential to evaluate different systems or architectures. This research allows the implementation of six different propulsion architectures and the exploration of the impact of design challenges on the vehicle. This type of modularity is only possible with a flexible environment. The flexibility characteristic enables the integration of legacy codes with experimental data and physics-based models. Furthermore, the flexibility of the environment also makes possible the integration of detailed mission analysis modules. Flying the mission directly with the disciplinary analysis results allows the exploration of operational challenges like a hurricane-tracking mission.

To demonstrate the capabilities of the design environment, the Pathfinder Plus vehicle was modeled from publicly available data. A case study explored the feasibility of two propulsion architectures to perform a hurricane-tracking mission. Furthermore, surrogate models derived from the environment were used to optimize the vehicle baseline configuration, explore the vehicle design space and consequently fly a notional hurricane-tracking mission.

As future work, it is planned to improve the structural module to account for more complex internal wing layout and, consequently, calculate the wing mass directly from the module. A volumetric sizing is being considered to analyze different packaging options of the internal components of the vehicle. A cost model is needed to perform economics tradeoffs, resource allocation, and systems life cycle analysis. More thorough constraint analysis will be considered to better capture a range of performance requirements in the initial sizing. A fidelity management technique also needs to be developed to correct lower fidelity results with higher-fidelity tools and thereby gain many advantages of both. Finally, there are a range of uncertainty analysis techniques beyond Monte Carlo simulation that could be applied to the environment, thereby gaining insight into where higher-fidelity tools would be most useful in reducing uncertainty during the design process.

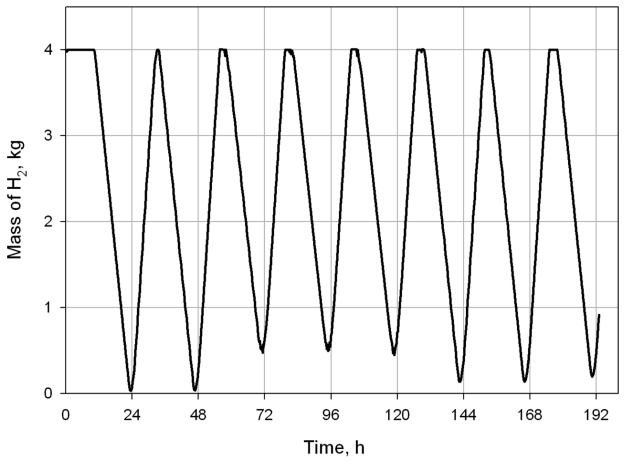

Fig. 20 Variation of the hydrogen mass.

Acknowledgments

The authors would like to thank the NASA Langley Research Center, more specifically Mark Guynn, for supporting this research under contract NAS 3-00179. The authors would also like to thank Mandy Goltsch, Matthew Prior, Hongjun Ran, and Reid Thomas for their contributions to the design environment disciplinary modules and Sriram Rallabhandi, Danielle Soban, and Nicholas Alley for their valuable comments.

References

[1] Herrick, K., "Development of the Unmanned Aerial Vehicle Market: Forecasts and Trends," *Air and Space Europe*, Vol. 2, No. 2, March–April 2000, pp. 25–27.

[2] "Unmanned Aerial Vehicles Roadmap 2002–2027," From the Office of the Secretary of Defense, U.S. Department of Defense (Acquisitions, Technology, and Logistics), Air Warfare, Dec. 2002, http://www.acq.osd.mil/usd/uav_roadmap.pdf [retrieved 22 May 2007].

[3] Moffitt, B. A., Bradley, T. H., Mavris, D., and Parekh, D. E., "Design Space Exploration of Small-Scale PEM Fuel Cell Long Endurance Aircraft," AIAA Paper 2006-7701, 2006.

[4] Moffitt, B., Bradley, T., Parekh, D., and Mavris, D., "Design and Performance Validation of a Fuel Cell Unmanned Aerial Vehicle," AIAA Paper 2006-823, 2006.

[5] Bradley, T. H., Moffitt, B., Thomas, R., Parekh, D. E., and Mavris, D., "Flight Test Results for a Fuel Cell-Powered Demonstration Aircraft," AIAA Paper 2007-32, 2007.

[6] Harmon, F. G., Frank, A. A., and Chattot, J., "Conceptual Design and Simulation of a Small Hybrid-Electric Unmanned Aerial Vehicle," *Journal of Aircraft*, Vol. 43, No. 5, 2006, pp. 1490–1498. doi:10.2514/1.15816

[7] Guynn, M., Croom, M., Smith, S., Parks, R., and Gelhausen, P., "Evolution of a Mars Airplane Concept for the ARES Mars Scout Mission," AIAA Paper 2003-6578, Sept. 2003.

[8] Wright, H., Croom, M., Braun, R., Qualls, G., Cosgrove, P., and Levine, J., "ARES Mission Overview: Capabilities and Requirements of the Robotic Aerial Platform," AIAA Paper 2003-6577, 2003.

[9] Rhew, R. D., Guynn, M. D., Yetter, J. A., Levine, J. S., and Young, L. A., "Planetary Flight Vehicles (PFV): Technology Development Plans for New Robotic Explorers," *AIAA InfoTech at Aerospace: Advancing Contemporary Aerospace Technologies and Their Integration*, Vol. 4, AIAA, Reston, VA, 2005, pp. 2058–2069; also AIAA Paper 2004-7132, 2004.

[10] McCullers, L. A., "FLOPS User's Guide, Release 6.12," revision 14, NASA Langley Research Center, Oct. 2004.

[11] Vanderplaats, G. N.,"Automated Optimization Techniques for Aircraft Synthesis," AIAA Paper 1976-0909, 1976.

[12] Jayaram, S., Myklebust, A., and Gelhausen, P., "ACSYNT: A Standards-Based System for Parametric Computer Aided Conceptual Design of Aircraft," AIAA Paper 1992-1268, 1992.

[13] Hague, D., "GASP-General Aviation Synthesis Program, Theoretical Development," Vol. 1 Main Program, Pt. 1, NASA Ames Research Center, CR 152303, Jan. 1978.

[14] Lu, Z., Yang, E. S., DeLautentis, D. A., and Mavris, D. N., "Formulation and Test of an Object-Oriented Approaches to Aircraft Design," AIAA Paper 2004-4302, 2004.

[15] Van Blyenburgh, P., "UAV Systems: Global Review," Avionics 2006 Conference Presentation, 9 March 2006.

[16] Neufeld, D. J., and Chung, J., "Unmanned Aerial Vehicle Conceptual Design Using a Genetic Algorithm, and Data Mining," AIAA Paper 2005-7051, 2005.

[17] Saleh, J. H., Hastings, D. E., and Newman, D. J., "Flexibility in System Design and Implications for Aerospace Systems," *Acta Astronautica*, Vol. 53, Elsevier, New York, 2003, pp. 927–944.
[18] Harmon, F. G., Frank, A. A., and Chattot, J., "Conceptual Design and Simulation of a Small Hybrid-Electric Unmanned Aerial Vehicle," *Journal of Aircraft*, Vol. 43, No. 5, 2006, pp. 1490–1498. doi:10.2514/1.15816
[19] Dolce, J., Colozza, A., and Wagner, R., "A Regenerative Electric Power System for High Altitude Airships," AIAA Paper 2003-6088, 2003.
[20] Snyder, D., and Memory, C., "A Modified Vortex Algorithm for Low Reynolds Number, Low Aspect-Ratio Wings," AIAA Paper 2005-4608, 2005.
[21] Phillips, W. F., "Modern Adaptation of Prandtl's Classic Lifting-Line Theory," *Journal of Aircraft*, Vol. 37, No. 4, 2000, pp. 662–670.
[22] Phillips, W. F., and Snyder, D. O., "Application of Lifting-Line Theory to Systems of Lifting Surfaces," AIAA Paper 2000-0653, 2000.
[23] Miranda, L., Elliott, R., and Baker, W., "A Generalized Vortex Lattice Method for Subsonic and Supersonic Flow Applications," NASA CR 2865, Nov. 1977.
[24] Petterson, K., "CFD Analysis of the Low-Speed Aerodynamic Characteristics of a UCAV," AIAA Paper 2006-1259, 2006.
[25] Iqbal, L., and Sullivan, J., "Application of an Integrated Approach to the UAV Conceptual Design," AIAA Paper 2008-144, 2008.
[26] Weisshaar, T. A., Nam, C., and Batista-Rodriguez, A., "Aeroelastic Tailoring for Improved UAV Performance," AIAA Paper 1998-1757, 1998.
[27] Garcia, J. A., "Numerical Investigation of Nonlinear Aeroelastic Effects on Flexible High-Aspect-Ratio Wings," *Journal of Aircraft*, Vol. 42, No. 4, 2005, pp. 1025–1036.
[28] Wang, Z., Chen, Z., Liu D., and Mook, D., "Nonlinear Aeroelastic Analysis for a HALE Wing Including Effects of Gust and Flow Separation," AIAA Paper 2007-2106, 2007.
[29] Vale, J., Lau, F., Suleman, A., and Gamboa, P., "Optimization of a Morphing Wing Based on Coupled Aerodynamic and Structural Constraints," AIAA Paper 2007-1890, 2007.
[30] Detrick, M., and Washington, G., "Modeling and Design of a Morphing Wing for Micro Unmanned Aerial Vehicles via Active Twist," AIAA Paper 2007-1788, 2007.
[31] Wu, Y.-T., Shin, Y., Sues, R. H., and Cesare, M. A.,"Safety-Factor Based Approach for Probability-Based Design Optimization," AIAA Paper 2001-1522, 2001.
[32] Verderaime, V., "Aerostructural Safety Factor Criteria Using Deterministic Reliability," *Journal of Spacecraft and Rockets*, Vol. 30, No. 2, 1993, pp. 244–247.
[33] Bhardwaj, M. K., Kapania, R. K., Reichenbach, E., and Guruswamy, G. P., "Computational Fluid Dynamics/Computational Structural Dynamics Interaction Methodology for Aircraft Wings," *AIAA Journal*, Vol. 36, No. 12, 1998, pp. 2179–2186.
[34] Yu, W., and Hodges, D., "The Timoshenko-Like Theory of the Variational Asymptotic Beam Sectional Analysis," AIAA Paper 2003-1419, 2003.
[35] "Systems Engineering Handbook, A "What To" Guide For All SE Practitioners," International Council on Systems Engineering TP-2003-016-02, Ver. 2a, June 2004.
[36] Cox, T. H., Nagy, C. J., Skoog, M. A., and Somers, I. A., "Civil UAV Capability Assessment," NASA, www.nasa.gov/centers/dryden/pdf/111761main_UAV_Capabilities_Assessment.pdf, 2004 [retrieved 30 May 2007].
[37] Green, L., Lin, H., and Khalessi, M., "Probabilistic Methods for Uncertainty Propagation Applied to Aircraft Design," AIAA Paper 2002-3140, 2002.
[38] Green, L., Alexandrov, N., Brown, S., Cerro, J., Gumbert, C., Sorokach, M., and Burg, C., "Decision Support Methods and Tools," AIAA Paper 2006-7028, 2006.
[39] Shishko, R., "NASA Systems Engineering Handbook," NASA SP 6105, 1995.
[40] Nam, T., "A Generalized Sizing Method for Revolutionary Concepts Under Probabilistic Design Constraints," Ph.D. Dissertation, Aerospace Department, Georgia Institute of Technology, Atlanta, GA, 2007.
[41] Price, M., Raghunathan, S., Curran, R., "An Integrated Systems Engineering Approach to Aircraft Design," *Progress in Aerospace Sciences*, Vol. 42, No. 4, 2006, pp. 331–376. doi:10.1016/j.paerosci.2006.11.002
[42] Drela, M., "XFOIL: An Analysis and Design System for Low Reynolds Number Airfoils," *Low Reynolds Number Aerodynamics*, Springer–Verlag, Berlin, June 1989, ISBN O-387-51884-3.
[43] Gloudemans, J. R., Davis, P. C., and Gelhausen, P. A., "A Rapid Geometry Modeler for Conceptual Aircraft," AIAA Paper 1996-52, 1996.
[44] Yu, W., Volovoi, V. V., Hodges, D. H., and Hong, X., "Validation of the Variational Asymptotic Beam Sectional Analysis," *AIAA Journal*, Vol. 40, No. 10, 2002, pp. 2105–2112.
[45] Raymer, D. P., "Vehicle Scaling Laws for Multidisciplinary Optimization: Use of Net Design Volume to Improve Optimization Realism," AIAA Paper 2001-5246, 2001.
[46] Romeo, G., and Frulla, G., "HELIPLAT: Aerodynamic and Structural Analysis of HAVE Solar Powered Platform," AIAA Paper 2002-3504, 2002.
[47] Mattingly, J. D., Heiser, W. H., and Daley, D. H., *Aircraft Engine Design*, 2nd ed., AIAA Education Series, AIAA, Reston, VA, 2002.
[48] "Pathfinder Fact Sheet," NASA, http://www.nasa.gov/centers/dryden/news/FactSheets/FS-034-DFRC.html [retrieved 6 July 2007].
[49] Laufer, A., Post, T., and Hoffman, E., "Flying High on Sprit: The Pathfinder Solar-Powered Airplane," *Shared Voyage: Learning and Unlearning from Remarkable Projects*, NASA History Division, NASA SP-2005-4111, 2005, ISBN 0-16-073240-9.
[50] Galante, N., "NASA Photo: ED02-0161-2," NASA Dryden Photo Collection, http://www.dfrc.nasa.gov/Gallery/photo/Pathfinder-Plus/index.html, June 2002 [retrieved 7 July 2007].
[51] Ehernberger, L. J., Donohue, C., and Teets, E., "A Review of Solar Powered Aircraft Flight Activity at the Pacific Missile Range Test Facility, Kauai, Hawaii," NASA Dryden Flight Research Center, 11th AMS Conference on Aviation, Range, and Aerospace Meteorology, http://ams.confex.com/ams/pdfpapers/82042.pdf [retrieved 4 Aug. 2007].
[52] Roskam, J., "Airplane Design Part VI: Preliminary Calculation of Aerodynamic, Thrust and Power Characteristics," Design, Analysis, and Research Corporation, Lawrence, KS, 2000, ISBN 1-8848-8552-7.
[53] Tschida, T., NASA Photo_EC04-0277-11, NASA Dryden Flight Research Center Photo Collection, http://www.dfrc.nasa.gov/Gallery/Photo/Pathfinder-Plus/Medium/EC04-0277-11.jpg [retrieved Jan. 2008].
[54] Hongjun, R., Thomas, R., and Mavris, D. N., "A Comprehensive Global Model of Broadband Direct Solar Radiation for Solar Cell Simulation," AIAA Paper 2007-33, 2007.
[55] Fatemi, N. S., Sharma, S., Buitrago, O., Crisman, J., Sharps, P. R., Blok, R., Kroon, M., Jalink, C., Harris, R., Stella, P., and Distefano, S., "Performance of High-Efficiency Advanced Triple-Junction Solar Panels for the Lilt Mission Dawn," IEEE, Paper 618-621, 2005.
[56] Anderman, M., "Brief Assessment of Improvements in EV Battery Technology Since the BTAP June 2000 Report," California Air Resources Board, 2003.
[57] Larminie, J., and Lowry, J., *Electric Vehicle Technology Explained*, Wiley, New York, 2003.
[58] DeLaurentis, D., Mavris, D., and Schrage, D., "System Synthesis in Preliminary Aircraft Design Using Statistical Methods," NASA CR-203326, Sept. 1996.
[59] Garcia, C., Chang, B., Johnson, D., Bents, D., Scullin, V., and Jakupca, I., "Round Trip Energy Efficiency of NASA Glenn Regenerative Fuel Cell System," NASA TM 2006-214054, 2006.
[60] Burke, K., "High Energy Density Regenerative Fuel Cell Systems for Terrestrial Applications," NASA TM 1999-209429, 1999.
[61] Mavris, D., DeLaurentis, D., Bandte, O., and Hale, M., "A Stochastic Approach to Multi-Disciplinary Aircraft Analysis and Design," AIAA Paper 98-0912, 1998.